

Ground State Phase Diagrams and Magnetic Properties of the Double Perovskite $\text{Pb}_2\text{FeReO}_6$

S. MTOUGUI¹, S. IDRISSE¹, H. LABRIM², N. EL MEKKAOUI¹, I. EL HOUSNI¹, S. ZITI³, R. KHALLADI¹ and L. BAHMAD^{1,*}

¹ Laboratoire de la Matière Condensée et des Sciences Interdisciplinaires (LaMCSdI), Mohammed V University of Rabat, Faculty of Sciences, B.P. 1014 Rabat, Morocco.

² USM/DERS/Centre National de l'Energie, des Sciences et des Techniques Nucléaires (CNESTEN), Rabat, Morocco.

³ Intelligence Artificial and Security of Systems, Mohammed V University of Rabat, Faculty of Sciences, B.P. 1014 Rabat, Morocco.

Abstract:

The Half-Metallic Ferromagnetic behavior of some double perovskites attracts much interest. In this work, we studied the magnetic behavior of the double perovskite $\text{Pb}_2\text{FeReO}_6$. The magnetic atoms are Fe and Re and have the spins $S=5/2$ and $\sigma=1$, respectively. In a first step, we provide a theoretical study of the ground state phase diagrams. In fact, we present and discuss the stable configurations from the all $6 \times 3 = 18$ possible configurations. Secondly, the magnetic properties of this compound when varying different physical parameters is carried out. Besides, we used Monte Carlo simulations (MCS), under the Metropolis algorithm to provide the magnetic behavior of the studied system as a function of the temperature, the crystal field, the exchange coupling interactions and the external magnetic field. In addition, we studied and discussed the critical temperature of the double perovskite $\text{Pb}_2\text{FeReO}_6$. To complete our study, we presented and analyzed the hysteresis loops for specific values of physical parameters.

Keywords: Double Perovskite; $\text{Pb}_2\text{FeReO}_6$; Mixed Spin; Monte Carlo Simulations; Hysteresis Cycles; Critical Temperature.

*) Corresponding authors: bahmad@fsr.ac.ma (L.B.); sara.mtougui@gmail.com (S.M.)

I. Introduction

Recently, the perovskites with mixed-metal oxides have attracted much interest for industrial and photovoltaic applications because of their low price, adaptability, and thermal stability. Such materials have shown interesting magnetic and optical properties [1].

During the years 1998 and 1999, Kobayashi *et al.* [2, 3] discovered the half-metallic ferromagnetic (HM-FM) properties, the large tunneling magnetoresistance (TMR) and high Curie temperature (T_c) for the compounds $\text{Sr}_2\text{FeMoO}_6$ and $\text{Sr}_2\text{FeReO}_6$, respectively. The HM-FM behavior has also been detected in many double perovskites such as $\text{Ho}_2\text{NiMnO}_6$ [4], $\text{Ba}_2\text{CrMoO}_6$ and $\text{Ba}_2\text{FeMoO}_6$ [5]. Additionally, these compounds present 100% spin polarization of the conduction electrons at the Fermi level and contribute to the development of technological applications in the devices of single-spin electron source and high-efficiency magnetic sensors [6, 7]. Moreover, recent works have been motivated the study of the double perovskite compounds with a general chemical formula $\text{A}_2\text{MM}'\text{O}_6$; where A is an alkaline-earth metal atom or rare earth metal atom, M stand for the 3d transition-metal (TM) atom and M' is the 4d/5d TM atom [8]. The majority of the double perovskites have been found to take a rock-salt crystal structure alternating perovskite units AMO_3 and $\text{AM}'\text{O}_3$ along three crystallo-graphical axes. The corners of each perovskite unitary alternately are occupied by the TM atoms M and M'. The oxygen atoms are located between M and M' atoms forming alternate MO_6 and $\text{M}'\text{O}_6$ octahedra. The large alkaline-earth-metal atom or rare-earth-metal atom A occupies the body-centered site with a (12-fold) oxygen coordination in each unit [9].

The combinations of the atoms A, M and M' can be chosen depending on the desired applications. For spintronic devices $\text{Sr}_2\text{FeMoO}_6$ [2] and $\text{Sr}_2\text{FeReO}_6$ [3] represent good examples, for multiferroicity to quote the $\text{Ba}_2\text{NiMnO}_6$ [10], in magneto-dielectric materials $\text{La}_2\text{NiMnO}_6$ [11, 12] and in magneto optic applications $\text{Sr}_2\text{CrReO}_6$ and $\text{Sr}_2\text{CrOsO}_6$ [13].

During the year 2009, Nishimura *et al.* [14] elaborated a new interesting double perovskite, $\text{Pb}_2\text{FeReO}_6$. Earlier, in 2001, Wolf *et al.* [12] presented the importance of thin films of $\text{Pb}_2\text{FeReO}_6$ sandwiching a thin nonmagnetic film (Cu film in spin valve device) or a very thin insulating layer (Al_2O_3 film in magnetic tunnel junction device). So maintaining the HM-FM behavior of the $\text{Pb}_2\text{FeReO}_6$ thin films is interesting for technological applications in magneto resistive and spintronic devices [9].

Experimentally, the double perovskite $\text{Pb}_2\text{FeReO}_6$ was prepared under the special conditions of pressure 6 GPa and temperature 1000 °C. The synchrotron X-ray powder diffraction study,

showed that this perovskite crystallizes in the tetragonal structure ($a = b = 5.62 \text{ \AA}$ and $c = 7.95 \text{ \AA}$) belonging to the space group $I4/m$ with the presence of Pb^{2+} ions at the A site. At temperatures less than 23 K, no structural transition to the lower symmetry was recorded. This perovskite displayed a ferromagnetic transition at 420 K [14]. The Curie temperature (T_c) of this perovskite is about 420 K; this value is slightly higher than that one of $\text{Sr}_2\text{FeReO}_6$, which is about 401 K [15]. The distances between the four equatorial metal transitions and oxygen are less than they are in the two axial transitions. Also, this compound shows the existence of the Jahn–Teller structural distortion in FeO_6 and ReO_6 octahedra [16]. The Fe^{3+} ions are in the states $3d^5$ with the magnetic moment of spin $S=5/2$ and Re^{5+} ions are in the states $5d^2$ with the magnetic moment of spin $\sigma=1$. The magnetic moments of Fe^{3+} and Re^{5+} are 3.929 and $-0.831 \mu_B$, respectively. Therefore, there exists an anti-ferromagnetic (AFM) coupling via oxygen between these two ions [16]. The half-metallic ferromagnetic (HM-FM) behavior exhibits a potential application of this new compound in magneto electronic and spintronic devices [16]. In one of our recent works [17], we have studied and discussed the magnetic properties of the perovskite BiFeO_3 , showing the hysteresis loops of this compound.

Motivated by the above considerations, the aim of this paper is to study and predict the phases diagrams and the magnetic properties of the double perovskite $\text{Pb}_2\text{FeReO}_6$, using Monte Carlo simulations (MCS). In a first step, we perform the ground state phase diagrams for the perovskite $\text{Pb}_2\text{FeReO}_6$; then we explore the effect of physical parameters, such as the temperature, the exchange coupling interactions, the crystal field and the external magnetic field on the behavior of the total magnetizations and susceptibilities. In addition, the behavior of the hysteresis loops for specific values of the physical parameters has been carried out. To achieve this goal, we will provide the ground state phase diagrams and the obtained results of Monte Carlo Simulations. This method is based on computer simulations under the Metropolis algorithm, often used to solve difficult physical problems [18–22]. The geometry of the double perovskite $\text{Pb}_2\text{FeReO}_6$ has been established using the Vesta software [23]. The critical exponents of this double perovskite $\text{Pb}_2\text{FeReO}_6$ have been established using the well-known finite-size scaling functions [24–28].

In some of our recent works, we have applied both the Monte Carlo simulations and Ab-initio approach, in order to investigate and discuss the magnetic properties of some multi-ferroic alloys [29–32].

This paper is organized as following. In Section II, we present the physical model. In section III, we discuss the obtained results. We finally complete this work with a conclusion in section IV.

II. Theoretical model

To study the behavior of such complex spin systems, we used Monte Carlo Simulations. This method showed its efficacy in the study of magnetic behavior of magnetic materials [33, 34]. The studied compound consists of two interpenetrating sub-lattices. One sublattice has spins σ and the other sublattice has spins S . The spins S have the spins σ and spins S as nearest neighbors and vice versa. The geometry of the studied system is belonging to the space group $I4/m$ (No. 87), and is displaying in (Fig. 1). In this figure, the left side illustrates the total crystallographic structure; the right side shows only the magnetic structure atoms. The double perovskite $\text{Pb}_2\text{FeReO}_6$ exhibits a similar magnetic origin to that of $\text{Sr}_2\text{FeMoO}_6$ [35].

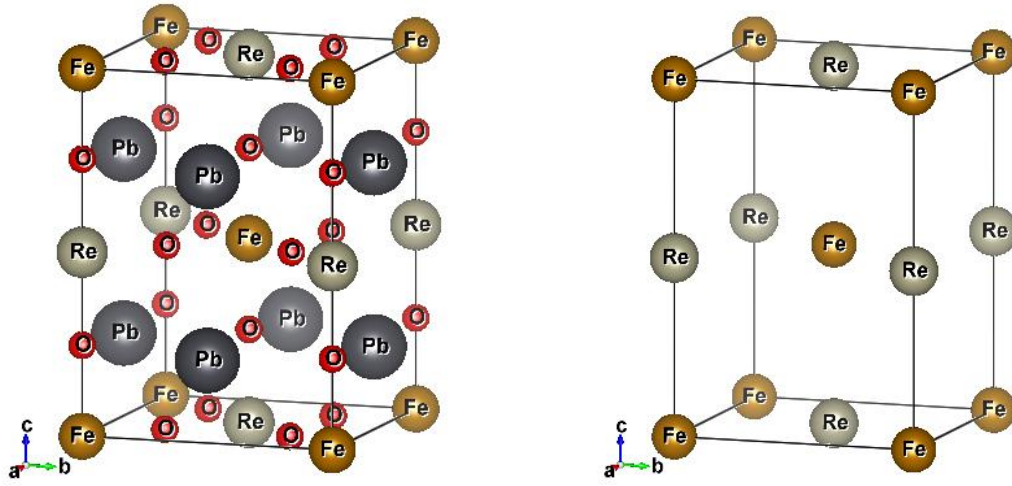


Figure 1. The geometry of the $\text{Pb}_2\text{FeReO}_6$ using Vesta software [23]. In left side Crystallographic structure, in right side only magnetic structure.

The Re sublattice has spins σ and takes the values ± 1 and 0, the Fe sublattice has spins S that can takes six values: $\pm 5/2$, $\pm 3/2$ and $\pm 1/2$. Based on Ising model, the Hamiltonian controlling this system is as following:

$$\mathcal{H} = -J_1 \sum_{\langle i,j \rangle} S_i S_j - J_2 \sum_{\langle k,l \rangle} \sigma_k \sigma_l - J_3 \sum_{\langle m,n \rangle} S_m \sigma_n - D_S \sum_i S_i^2 - D_\sigma \sum_i \sigma_i^2 - H(\sum_i (S_i + \sigma_i)) \quad (1)$$

The notation $\langle i, j \rangle$, $\langle k, l \rangle$ and $\langle m, n \rangle$ stand for the first nearest-neighbors spins. We performed and combined a MCS with Metropolis algorithm to simulate the magnetic behavior of this system.

J1: the interaction coupling between the nearest neighbors of Fe-Fe atoms ($J_1=0.89$ eV [8]).

J2: the interaction coupling between the nearest neighbors of Re-Re atoms ($J_2=0.89$ eV [8]).

J3: the interaction coupling between the nearest neighbors of Fe-Re atoms ($J_3=0.89$ eV [8]).

D_S and D_σ : represent the crystal fields of the two sub-lattices Iron and Rhenium, respectively. The origin of this field is the competition between Fe–O and Re–O interactions in the compound. For reason of simplicity, we make $D = D_S = D_\sigma$ ($D=3$ eV [8]). H is the external magnetic field.

Table 1. Coordinates of Pb_2FeReO_6 [14].

Site	Location	X	Y	Z
Pb	8g	0.000	0.500	0.2244 (1)
Fe1	2a	0.000	0.000	0.000
Fe2	2b	0.000	0.000	0.500
Re1	2a	0.000	0.000	0.000
Re2	2b	0.000	0.000	0.500
O1	8h	0.246(15)	0.252(11)	0.000
O2	4e	0.000	0.000	0.247(17)

III. Monte Carlo Simulation

In this study, we investigate the magnetic properties of the perovskite Pb_2FeReO_6 using MCS. The magnetic structure is based on the position of the magnetic atoms, which are identified with Iron (Fe) and Rhenium (Re). This computation is founded on the Hamiltonian given in Eq. (1). For every spin configuration, 10^5 Monte Carlo steps are performed. At each MCS step, all the sites in the system are visited and single-spin flip attempts are made. The flips are accepted or rejected according to the probability based on the Boltzmann statistics. The free boundary conditions are applied for the super cell lattice size $5 \times 5 \times 5$.

At equilibrium, averages of the energy, the partial-total magnetizations and the partial-total magnetic susceptibility of the system have been calculated. We calculate, on each iteration, the internal energy per site (Eq.2). Afterward, we determinate the magnetization and we finally extract the magnetic susceptibility.

The internal energy:

$$E = \frac{\langle \mathcal{H} \rangle}{N_T} \quad (2)$$

Where $N_T = N_\sigma + N_S$ is the total numbers of spins in the super-cell unit, N_σ being the number of σ spins and N_S is the total number of S spins.

The partial magnetizations are calculated as follows:

$$M_S = \langle \frac{1}{N_S} \sum_i S_i \rangle \quad (3)$$

$$M_\sigma = \langle \frac{1}{N_\sigma} \sum_i \sigma_i \rangle \quad (4)$$

The total magnetization is given by:

$$M_T = \frac{N_S M_S + N_\sigma M_\sigma}{N_T} \quad (5)$$

The partial and total susceptibilities are given by:

$$\chi_S = \frac{\langle M_S^2 \rangle - \langle M_S \rangle^2}{K_B T} \quad (6)$$

$$\chi_\sigma = \frac{\langle M_\sigma^2 \rangle - \langle M_\sigma \rangle^2}{K_B T} \quad (7)$$

$$\chi_T = \frac{\langle M_T^2 \rangle - \langle M_T \rangle^2}{K_B T} \quad (8)$$

Where K_B is the Boltzmann constant fixed at the value: $K_B=1$ and T being the absolute temperature.

IV. Results and discussion

In this section, we analyze and discuss the ground states phase diagrams of the double perovskite $\text{Pb}_2\text{FeReO}_6$ at vanishing temperature ($T = 0$ K). Hence, we provide interpretations of the effect of physical parameters on the magnetizations and the susceptibilities.

IV.1. Study of the ground state phases

In this part, we study the ground state phase diagrams indifferent plans in order to establish and discuss the all-possible configurations. Using the Hamiltonian of Eq.(1), we computed the energies of all possible $6 \times 3 = 18$ configurations. Figs. 2.a, ..., 1.f show the obtained results in different planes corresponding to different physical parameters. Indeed, Fig. 2.a illustrates the twelve stable configurations plotted in the plane (J_1, J_2) for $J_3 = -1$, in the absence of both magnetic external and crystal fields ($H = D = 0$). These twelve stable phases are: $(\pm 1/2, \pm 1)$, $(\pm 3/2,$

± 1), $(\pm 5/2, \pm 1)$. In fact, a perfect symmetry is present in this figure regarding the axis ($J_2 = -5$) when varying the parameter J_1 . For the specific point ($J_2 = -5, J_1 = -5$), we note the coexistence of all stable phases. This is due to the competition between the different exchange coupling interactions for the magnetic spins $S = 5/2$ and $\sigma = 1$.

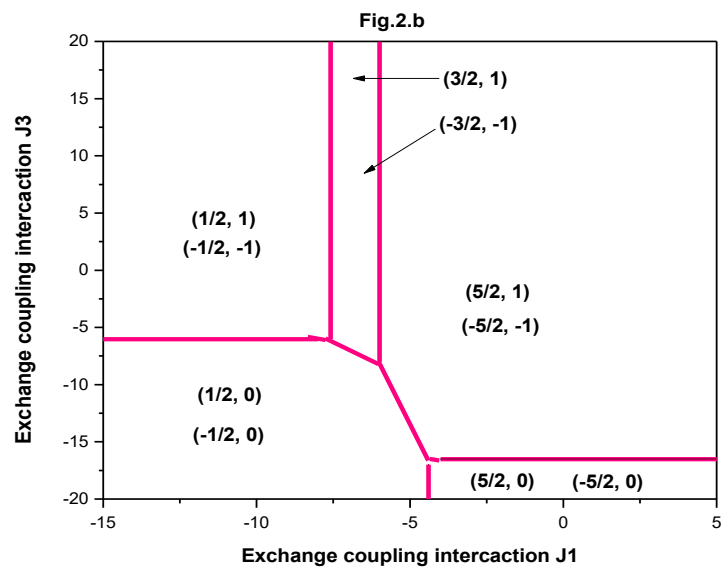
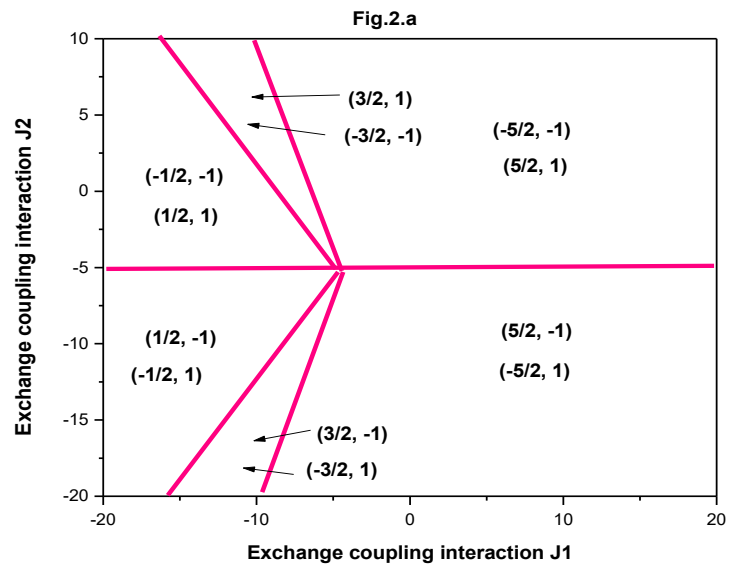
In Fig. 2.b, plotted in the plane (J_1, J_3) for $J_2 = -1$, we found that the phases $(\pm 1/2, 0)$ and $(\pm 5/2, 0)$ are appearing for the crystal field value ($D = 0$) and the magnetic external field ($H = 0$). These phases are stable only for negative and large values of the parameter J_3 .

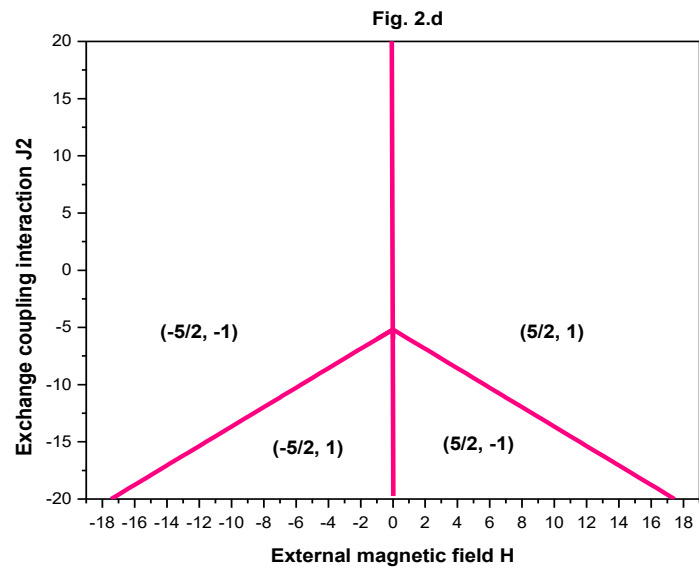
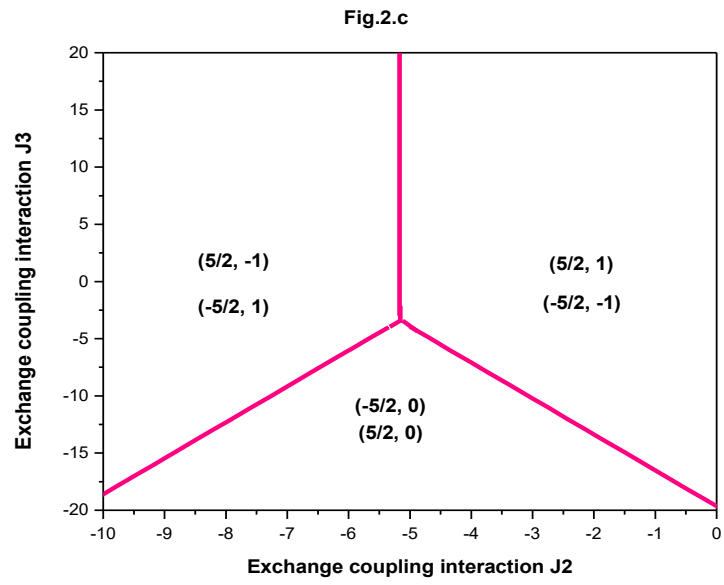
When fixing the interaction between Fe-Fe atoms ($J_1 = -1$), the Fig. 2.c shows the corresponding stable configurations plotted in the plane (J_2, J_3). There is only six stable configurations, namely: $(\pm 5/2, 0)$ and $(\pm 5/2, \pm 1)$. When varying the exchange coupling interaction J_2 between Re-Re atoms, and keeping that one between Fe-Fe atoms at the fixed value of $J_1 = -1$, the extremely values of the magnetic moments of spin of Fe ($S = \pm 5/2$) are found to be stable in this figure. Similarly, the stable phases shown in Fig. 2.d are still found to keep the extremely values for the both spins S and σ , namely: $\pm 5/2$ and ± 1 , respectively.

In Fig. 2.d, plotted in the plane (H, J_2) for $J_1 = J_3 = -1$ and $D = 0$, we found that only four stable configurations are present in this figure, namely: $(\pm 5/2, \pm 1)$. A perfect symmetry is found in this figure regarding the axis $H = 0$. Also, the sign of each stable configuration is the same as that one of the external magnetic field. This means that the stable configurations with positive values are found for positive H values and vice-versa.

To inspect the effect of both the magnetic external and the crystal fields on the stable configurations, we illustrate in Fig. 2.e plotted in the plane (H, D), the obtained results for the fixed values of $J_1 = J_2 = J_3 = -1$. From this figure, we note that the increasing crystal field values effect is to allow the apparition of the eight stable phases: $(-5/2, -1)$, $(5/2, 1)$, $(-3/2, -1)$, $(-1/2, -1)$, $(-1/2, 0)$, $(1/2, 0)$, $(1/2, 1)$, $(3/2, 1)$. A perfect symmetry is present in this figure, according to the axis $H = 0$. Also, it is found that for large and positive values of the crystal field, the only stable phases are those corresponding to the extreme moment of spin values: $\pm 5/2$ and ± 1 , respectively.

To complete this ground state phase diagram discussion, we provide the stable phases in Fig. 2.f, plotted in the plane (D, J_1) for $H = 0$ and $J_2 = J_3 = -1$. From this figure, it is clear that the only stable phases are those already found in the other phase diagrams, namely: $(\pm 5/2, 0)$, $(\pm 1/2, 0)$, $(-5/2, 1)$, $(5/2, -1)$, $(-1/2, 1)$ and $(1/2, -1)$. It is worth to note that each configuration and its opposite are both stable in each region of this figure, see Fig. 2.e.





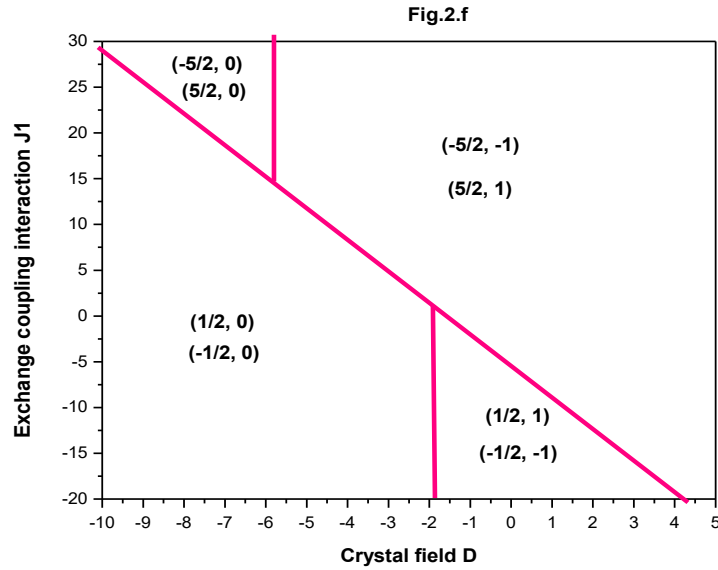
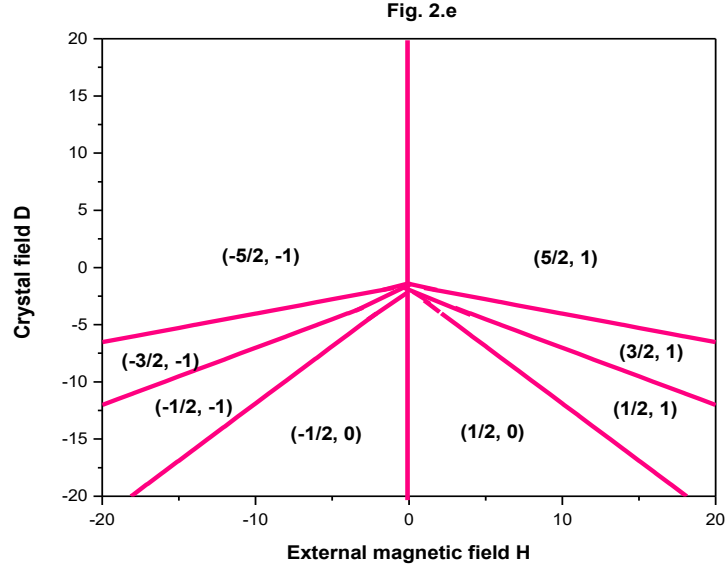


Figure 2. Ground phase state diagrams of the compound $\text{Pb}_2\text{FeReO}_6$ in different planes: (a) in the plane $(J1, J2)$ for $J3=-1$, in the absence of both magnetic external and crystal fields ($H=D=0$); (b) in the plane $(J1, J3)$ for $J2=-1$ and $H=D=0$; (c) in the plane $(J2, J3)$ for $J1=-1$ and $H=D=0$; (d) in the plane $(H, J2)$ for $J1=J3=-1$ and $D=0$; (e) in the plane (H, D) $J1=J2=J3=-1$ and (f) in the plane $(D, J1)$ for $H=0$ and $J2=J3=-1$.

IV.2. Monte Carlo Simulations

In order to study the critical properties of the compound $\text{Pb}_2\text{FeReO}_6$, we perform Monte Carlo simulations under Metropolis algorithm. In fact, such calculations are performed based on the Hamiltonian given in Eq. (1). At each spin configuration, a number of 10^5 Monte Carlo steps

are performed. When running a Monte Carlo simulation, we discard the first 10^4 generated configurations. Single-spin flip attempts are made and the all sites of the system are visited. The flips are accepted or rejected according to the well-known probability of the Boltzmann statistics.

The obtained results are presented in Fig. 3, showing the total magnetization and susceptibility as a function of temperature for $H=0$, $D=3$, $J_1=J_2=J_3=0.89$. From this figure, for low temperature values, the total magnetization reaches the exact value $M_T=1.75$, in good agreement with the value of the ground state which is $M_T=(5/2+1)/2$ for the fixed values $D=3$, $J_1=J_2=J_3=0.89$. The total magnetization decreases when increasing the temperature. The total susceptibility reaches its maximum at the transition temperature corresponding to $T_c=15$ K, and changes its behavior above this point.

The behavior of the total magnetization as a function of crystal field is illustrated in Figs. 4.a, 4.b and 4.c, for $H=0$, selected values of the other physical parameters. In Fact, Fig. 4.a shows such behavior for selected temperature values: $T=0.01, 5$ and 10 K. From this figure, it is found that for low values of crystal field $D \leq -5$, there are no crystal field effect on the attitude of the total magnetization. However, the effect of the crystal field in the region $-5 \leq D \leq 5$ is to decrease abruptly the total magnetization. Beyond the crystal field value $D>5$, the total magnetization reaches rapidly the saturation value $M_T=1.75$. The pertinent parameter here is the crystal field effect since the changing sign of this parameter leads to a brutal change of the total magnetization behavior. The effect of varying the exchange coupling interaction between J_3 between Re-Fe atoms is illustrated in Fig. 4.b, for the values $J_3=+3, -3$ and -1 . It is found that the total magnetizations are strongly affected by the J_3 variations in the interval of the crystal field $-5<D<+5$. Outside this interval, for high values of the crystal field, the total magnetizations are not affected by the variations of the parameter J_3 , see Fig. 4.b.

When varying the exchange coupling interaction between J_1 between Fe-Fe atoms, the behavior of the total magnetizations is presented in Fig. 4.c for the specific values: $J_1=+3, -3$ and -1 . Similarly to Fig. 4.b, outside the interval $-5<D<+5$, the total magnetizations are slightly affected by the variations of the parameter J_1 .

The behavior of the total magnetization as a function of the magnetic external field is illustrated in Figs. 5.a,..., 5.d. In all the following figures, the magnetization behavior of the antiferromagnetic and the ferromagnetic films causes a shift in the soft magnetization curve, this phenomena is due to the exchange bias effect, see for example Refs. [36-38]. In Fig. 5.a,

we present such behavior for different temperature values: $T=0.01, 5$ and 10 K. As it is expected, the surface of the hysteresis loops decreases when increasing the temperature values. The corresponding coercive field also decreases when the temperature increases. The effect of varying the crystal field when increasing the external magnetic field is illustrated in Fig. 5.b, for $D=+3, -3$ and 0 . Contrary to the temperature effect, the effect of increasing the crystal field is to increase both the surface and the corresponding coercive field of the loops.

To inspect the effect of varying both the parameters $J1$ and $J3$ are presented in Fig. 5.c and Fig. 5.d, respectively. In fact, Fig. 5.c is devoted to the variation of the total magnetization as a function of the magnetic external field for $J1=+1, -1$ and -3 . The hysteresis surface loops are practically not affected by the increasing values of the exchange coupling interaction between Fe-Fe atoms $J1$.

In Fig. 5.d, plotted for $J3=+1, -1$ and -3 , we show the effect of varying the exchange coupling interaction between Re-Fe atoms on the hysteresis loops. For $3=+1$, there is apparition of intermediate steps, probably due to the low interaction between Re-Fe atoms.

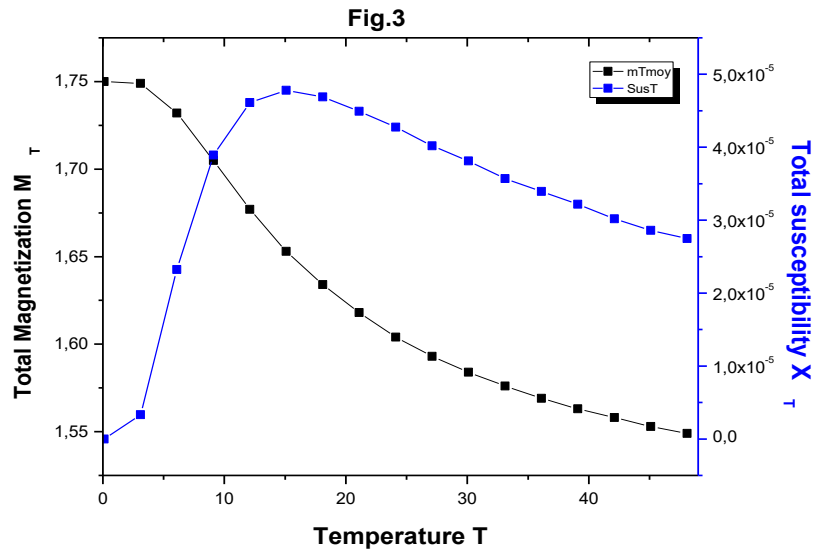


Figure 3. Total Magnetization and total susceptibility as a function of temperature for $H=0$, $D=3$ and $J1=J2=J3=0.89$.

Fig.4.a

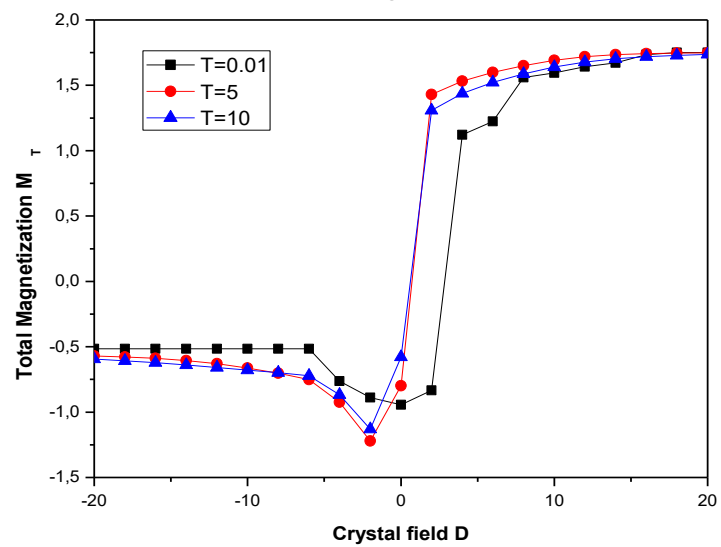
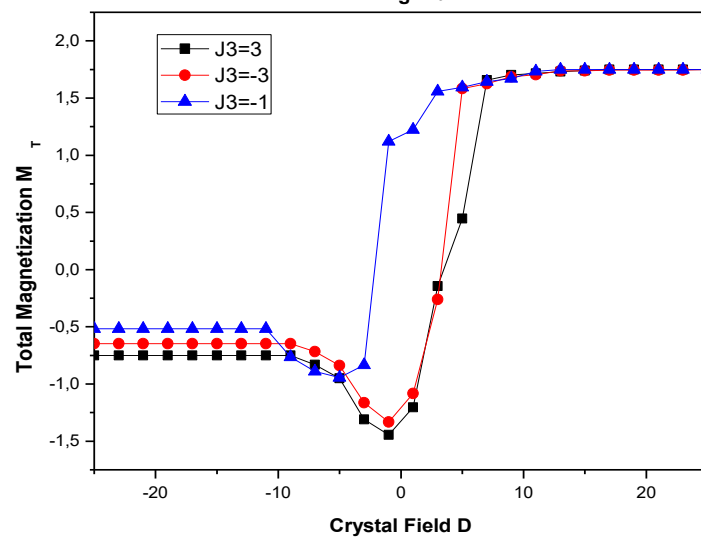


Fig.4.b



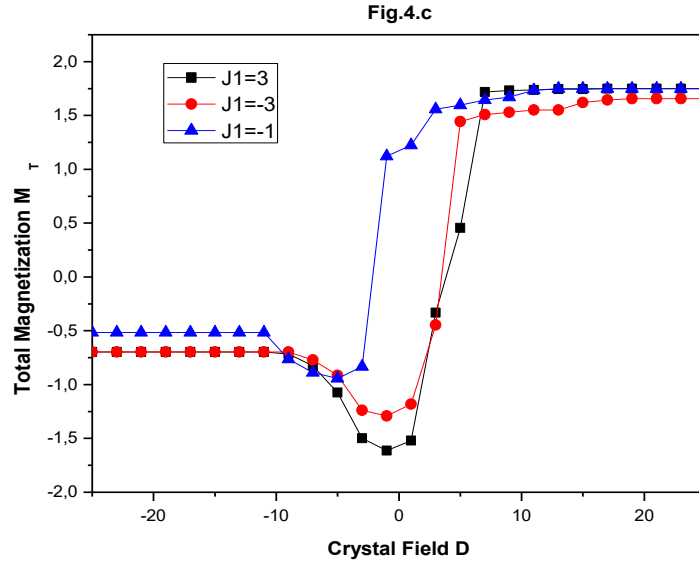


Figure 4. Total magnetization as a function of crystal field for $H=0$: in (a) for $J1=J2=J3=-1$, and $T=0.01, 5$ and 10 K; in (b) for $T=0.01$ K, $J1=J2=-1$ and $J3=+3, -3$ and -1 ; in (c) for $T=0.01$ K, $J2=J3=-1$ and $J1=+3, -3$ and -1 .

Fig.5.a

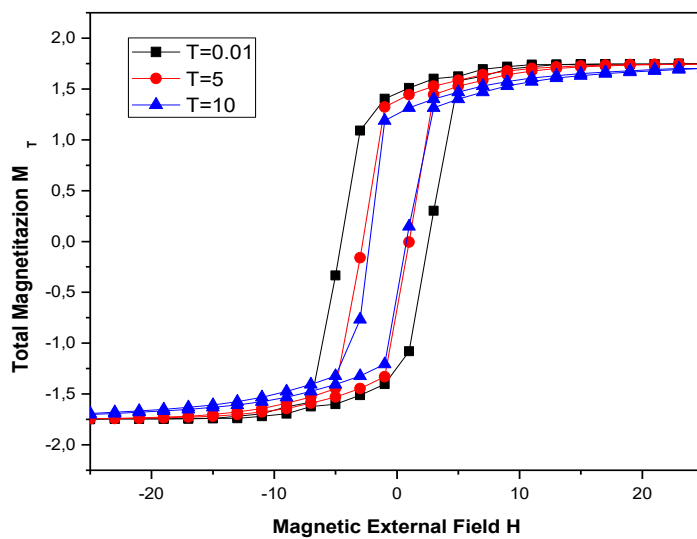
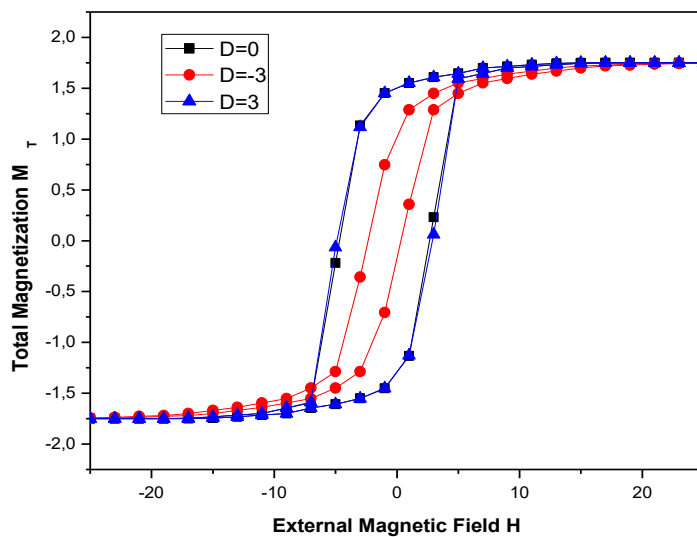


Fig.5.b



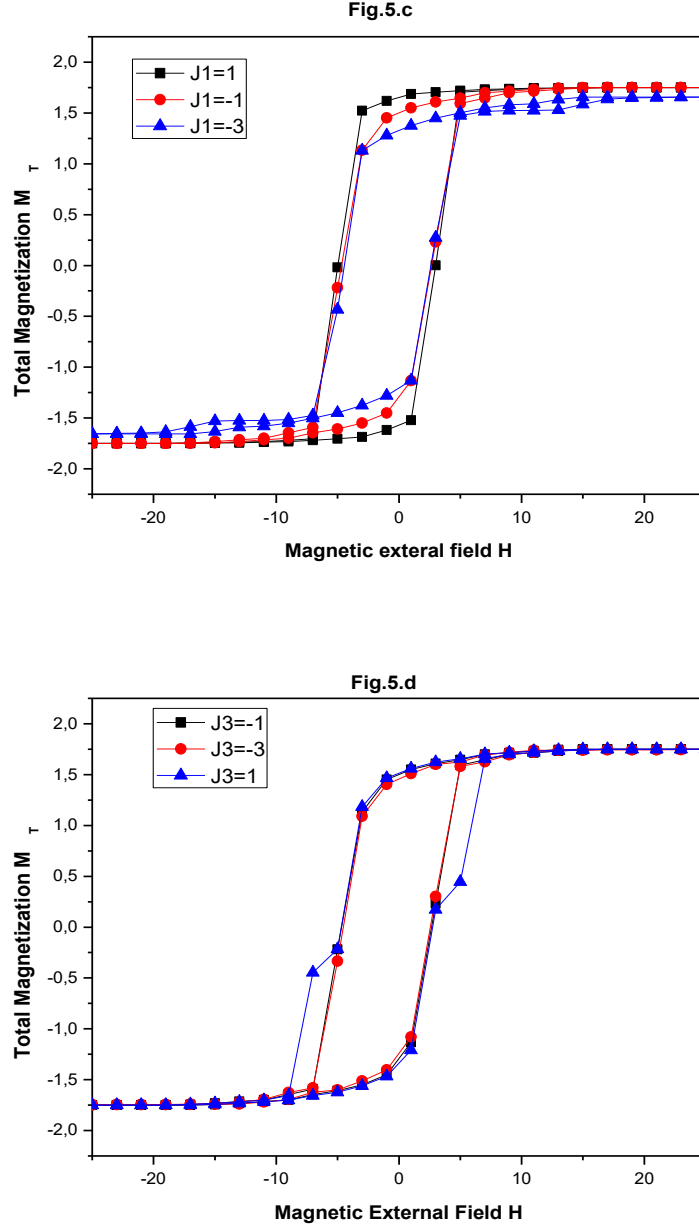


Figure 5. Total Magnetization vs. magnetic external field: in (a) for $J1=J2=J3=-1$, $D=0$ and $T=0.01K$, 5 and 10 K; in (b) for $J1=J2=J3=-1$, $T=0.01$ and $D=+3$, -3 and 0; in (c) for $J2=J3=-1$, $D=0$, $T=0.01K$ and $J1=+1$, -1 and -3 ; in (d) for $J1=J2=-1$, $D=0$, $T=0.01K$ and $J3=+1$, -1 and -3 .

V. Conclusion

Using the Monte Carlo simulations (MCS) we have inspected and predicted the phase diagrams and the magnetic properties of the half-metallic double perovskite Pb_2FeReO_6 . To define the stable states between the $6 \times 3 = 18$ possible configurations, based on the Hamiltonian of this system in the absence of any temperature, we calculated the energy corresponding to every

configuration and taken the minimum one. The more stable configurations are; $(-5/1, -1)$ and $(5/2, 1)$, they coexist in all planes. On the other hand, we have examined the behavior of the total magnetizations and the total susceptibilities as a function of the temperature, the crystal field, the exchange coupling interactions and the external magnetic field. To complete this study, we analyzed and discussed the hysteresis loops for fixed values of temperature and the other physical parameters. It is found that for positive values of the exchange coupling interaction J_1 between Fe-Fe atoms, the maximum value of the total magnetization ($M_T=1.75$) is reached rapidly. On the other hand, we found that increasing the crystal field and the exchange coupling interaction values lead to increase the surface, the corresponding coercive field and the remanent magnetization of the loops. Moreover, by increasing the temperature, the surface, the coercive field and the remanent magnetization of the loops decrease. The temperature of transition is found to be about $T_C=11$ k for the fixed physical parameters.

References:

- [1] N. Labhasetwar et al, Perovskite-type catalytic materials for environmental applications, Sci. Technol. Adv. Mater. **16** (2015) 036002, doi:10.1088/1468-6996/16/3/036002.
- [2] K. I. Kobayashi, T. Kimura, H. Sawada, K. Terakura, Y. Tokura, Nature (London) **395** (1998) 677.
- [3] K. I. Kobayashi, T. Kimura, Y. Tomioka, H. Sawada, K. Terakura, Y. Tokura, Phys. Rev. B **59** (1999) 11159.
- [4] Chakraborty T, Nair HS, Nyhalil H, Kumar K R, Strydom A M, Elizabeth S. J Phys Condens Matter. 29 (2017) 025804.
- [5]. Musa Saad H-E M, El-Hagary M. J Magn Magn Mater. **360** (2014) 229.
- [6] Prinz G A., Magnetoelectronics, Science. **282** (1998) 1660. DOI: 10.1126/science.282.5394.1660
- [7] Wolf S A, Awschalom D D, Buhrman R A, et al. Science 294 (2001) 1448.
- [8] Y. Zhang et al. ‘Structural, electronic and magnetic properties of the double perovskite $\text{Pb}_2\text{FeReO}_6$ ’. Physica B **407** (2012) 2617. DOI: <http://dx.doi.org/10.1016/j.physb.2012.04.007>.

- [9] Y. Zhang et al., Structural, electronic, and magnetic properties of double perovskite $\text{Pb}_2\text{FeReO}_6$ thin films with (001) orientation and three possible terminations, *Surface and Interface Analysis*, *Surf. Interface Anal.*, **49** (2017) 1–7. DOI: 10.1002/sia.6252.
- [10] M. Azuma, K. Takata, T. Saito, S. Ishiwata, Y. Shimakawa, M. Takano, *J. Am. Chem. Soc.* **127** (2005) 8889.
- [11] N. S. Rogado, J. Li, A. W. Sleight, M. A. Subramanian, *Adv. Mater.* **17** (2005) 2225.
- [12] H. Das, U. V. Waghmare, T. Saha-Dasgupta, D. D. Sarma, *Phys. Rev. Lett.* **100** (2008) 186402.
- [13] H. Das, M. De Raychaudhury, T. Saha-Dasgupta, *Appl. Phys. Lett.* **92** (2008) 201912.
- [14] Nishimura et al., Synthesis and Physical Properties of Double Perovskite $\text{Pb}_2\text{FeReO}_6$, *Inorganic Chemistry*, Vol. **48**, No. 13, (2009) 5962.
- [15] Kobayashi K I, Kimura T, Tomioka Y, Sawada H, Terakura K, Tokura Y. *Phys. Rev. B.* **59** (1999) 11159.
- [16] Y. Zhang et al., Structural, electronic and magnetic properties of the double perovskite $\text{Pb}_2\text{FeReO}_6$, *Physica B* **407** (2012) 2617. <http://dx.doi.org/10.1016/j.physb.2012.04.007>.
- [17] S. Mtougui, R. Khalladi, S. Ziti, H. Labrim and L. Bahmad, Magnetic Properties of the Perovskite BiFeO_3 : Monte Carlo Simulation, Superlattices and Microstructures, **123**, (2018), Pages 111-118. doi: 10.1016/j.spmi.2018.05.005.
- [18] P. Landau, K. Binder, *A Guide to Monte Carlo Simulations in Statistical Physics*, Cambridge University Press, New York, NY, USA, (2005).
- [19] S. Sidi Ahmed, M. Boujnah, L. Bahmad, A. Benyoussef, A. El Kenz. Magnetic and electronic properties of double perovskite $\text{Lu}_2\text{MnCoO}_6$: Ab-initio calculations and Monte Carlo simulation, *Chemical Physics Letters* **685** (2017) 191–197.
- [20] S. Naji, A. Benyoussef, A. El Kenz, H. Ez-Zahraouy, M. Loulidi, Monte Carlo study of phase transitions and magnetic properties of LaMnO_3 Heisenberg model, *Phys. Stat. Mech. Appl.* **391** (15) (2012) 3885–3894.
- [21] M. El Yadari, L. Bahmad, A. El Kenz, A. Benyoussef, Monte Carlo study of the double perovskite nano Sr_2VMoO_6 , *J. Alloy. Compd.* **579** (2013) 86–91.

- [22] L. Bahmad, R. Masrour, A. Benyoussef, Nanographene magnetic properties: a Monte Carlo study, *J. Supercond. Nov. Magn.* **25** (6) (2012) 2015–2018, <http://dx.doi.org/10.1007/s10948-012-1552-y>.
- [23] K. Momma and F. Izumi, "VESTA 3 for three-dimensional visualization of crystal, volumetric and morphology data," *J. Appl. Crystallogr.*, **44** (2011) 1272-1276.
- [24] K. Binder, D.W. Heermann, Monte Carlo Simulation in Statistical Physics: An Introduction, Springer, Berlin, New York, 2002.
- [25] J. M. Yeomans, Statistical Mechanics of Phase Transitions, Oxford University Press, New York, 1993.
- [26] E. Jeckelmann, Computational many-particle physics, in: H. Fehske, R. Schneider, A. Weiße (Eds.), *Lect. Notes Phys.*, Springer-Verlag, Heidelberg, **739** (2008).
- [27] G. Dimitri Ngantso, A. Benyoussef, A. El Kenz, *Curr. Appl. Phys.* **16** (2016) 211.
- [28] S. Sidi Ahmed et al., *Physics Letters A* **382** (2018) 186–192.
- [29] S. Idrissi, R. Khalladi, S. Mtougui, S. Ziti, H. Labrim, I. El Housni, N. El Mekkaoui, L. Bahmad, Magnetism and phase diagrams of the double perovskite $\text{Sr}_2\text{CrIrO}_6$: Monte Carlo simulations. *Physica A* (2019). <https://doi.org/10.1016/j.physa.2019.03.004>.
- [30] S. Idrissi, R. Khalladi, S. Ziti, N. El Mekkaoui, S. Mtougui, H. Labrim, I. El Housni, L. Bahmad, The electronic and magnetic properties of the rare earth-based quaternary Heusler compound LuCoVGe . *Physica B* **562**, 116–123 (2019). <https://doi.org/10.1016/j.physb.2019.03.018>.
- [31] Idrissi, S., Labrim, H., Ziti, S. et al. *Journal of Elec Materi* (2019). <https://doi.org/10.1007/s11664-019-07110-z>.
- [32] Idrissi, S., Bahmad, L., Ziti, S. et al. *Appl. Phys. A* (2019) 125: 306. <https://doi.org/10.1007/s00339-019-2580-2>.
- [33] S. Mtougui, R. Khalladi, N. El Mekkaoui, I. El Housni, S. Idrissi, L. Bahmad, S. Ziti and H. Labrim, Study of the magnetic properties of the perovskite CeFeO_3 : Monte Carlo Simulations, *Comput. Cond. Mat.* **17** (2018) e00329. <https://doi.org/10.1016/j.cocom.2018.e00329>.

- [34] S. Mtougui, R. Khalladi, N. El Mekkaoui, I. El Housni, S. Idrissi, S. Ziti, H. Labrim and L. Bahmad, Magnetic properties of the rare earth cerium orthochromite perovskite CeCrO_3 , *Comput. Cond. Mat.* Vol. **17** (2018) e00331. <https://doi.org/10.1016/j.cocom.2018.e00331>.
- [35] Erchidi Elyacoubi, A. S., Masrour, R., Jabar, A., Ellouze, M., & Hlil, E. K. (2018). Magnetic properties and magnetocaloric effect in double $\text{Sr}_2\text{FeMoO}_6$ perovskites. *Materials Research Bulletin*, 99, 132–135. doi:10.1016/j.materresbull.2017.10.037.
- [36] Folcke, E., Le Breton, J. M., Lefebvre, W., Bran, J., Lardé, R., Golkar, F., & Shield, J. E. (2013). Investigation of the magnetic properties of FeAu nanoclusters in a W matrix: Evidence for exchange-bias phenomenon. *Journal of Applied Physics*, 113(18), 183903. doi:10.1063/1.4803129
- [37] J. Y. Chen, Naganivetha Thiyagarajah, H. J. Xu, and J. M. D. Coey, *Applied Physics Letters* 104, 152405 (2014); doi: 10.1063/1.4871711
- [38] Lester Clinton barnsley, Exchange bias in manganese alloys with mixed magnetic behavior, Phd thesis, Griffith University, April (2012).